IOP Publishing Superconductor Science and Technology
Supercond. Sci. Technol. 31 (2018) 115010 (7pp) https://doi.org/10.1088/1361-6668/aade5b

Design, modelling and simulation of a monolithic high-T_c superconducting terahertz mixer

Xiang Gao[1], Ting Zhang[2], Jia Du[1] and Yingjie Jay Guo[2]

[1] CSIRO Manufacturing, PO Box 218, Lindfield, NSW 2070, Australia
[2] Global Big Data Technologies Centre, University of Technology Sydney, Ultimo, NSW 2007, Australia

E-mail: Xiang.Gao@csiro.au

Received 30 June 2018, revised 24 August 2018
Accepted for publication 3 September 2018
Published 12 October 2018

Abstract

This paper presents a novel concept and design of a full monolithic integrated high-T_c superconducting (HTS) Josephson junction terahertz (THz) harmonic mixer coupled with a circularly polarized (CP) antenna. The fully on-chip mixer device is very compact in size and utilizes the CP antenna to enhance the polarization orientation flexibility in coupling THz radiation. Electromagnetic simulations are carried out to optimize the coupling efficiency and axial ratio of the THz CP antenna, and the signal transmission and isolation characteristics of the monolithic circuit. An equivalent circuit model of the HTS THz mixer is then established and simulation is performed based on our previously measured step-edge Josephson junction characteristics to evaluate the device performance and validate the concept of design. The results show that a superior performance could be achieved from such a monolithic HTS mixer device, which is significantly better than any HTS THz harmonic mixers reported to date.

Keywords: terahertz mixer, high-T_c superconducting Josephson junction, monolithic integrated mixer, circularly polarized antenna, terahertz wireless communication

(Some figures may appear in colour only in the online journal)

1. Introduction

Ultrahigh bitrate wireless links are increasingly in demand for many practical applications, such as last-mile broadband wireless access, real-time transmission of high-definition video signals, and fast restoration of network connections after natural disasters [1, 2]. To accommodate these growing needs, communication carrier frequency has been pushed higher and higher towards sub-millimetre and terahertz (THz) bands. The considerable bandwidth of THz waves brings great benefits to wireless communications, such as overcoming the system capacity bottleneck. However, due to the limited source power and severe atmospheric attenuation at the THz bands, the receiver system must be very sensitive for reliable signal detection, particularly over longer communication ranges. High-T_c superconducting (HTS) Josephson junction mixers are promising candidates for THz communication receiver frontends due to their high sensitivity, wide bandwidth, and lower cryogenic cost compared to cooling low-T_c superconducting devices. Early demonstrations of HTS THz mixers were mostly achieved in temperature ranges below 20 K [3–6] and later at 58 K [7]. Recently, HTS THz mixers that operate up to 77 K have been demonstrated at CSIRO's laboratory [8–11] using a step-edge junction technology [12]. The best noise and conversion performance at 600 GHz band were achieved [13].

In this paper, we propose a completely new concept of a full monolithic integrated circularly polarized (CP) antenna-coupled HTS THz harmonic mixer that comprises not only the antenna but all other components including the diplexer and bias-tee on-chip. Due to the removal of resistive connection losses between components and better signal coupling design, a significant performance improvement is expected from such a design. We shall show in this paper, by modelling and simulation, that a significantly better mixer performance is indeed obtained based on the same Josephson junction parameters as that of the previously measured mixer [9, 10]. To the best of our knowledge, this is the first attempt of

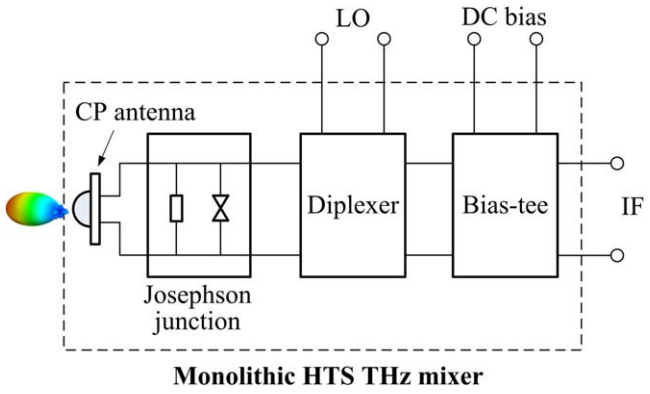

Figure 1. Schematic of the monolithic integrated CP antenna-coupled HTS Josephson junction THz harmonic mixer; all components in the dashed line box are integrated on-chip.

designing a full on-chip HTS THz mixer receiver. In addition to achieving the best device performance, such a monolithic integrated mixer configuration is hugely advantageous for constructing a compact cryogenic receiver and implementing a multi-channel architecture as a lower cooling power is required. In addition, the novel THz CP antenna greatly enhances polarization orientation flexibility while achieving high-efficiency radiation coupling. This is particularly useful for its application in moving platforms where the polarization orientation constantly varies. A detailed device design, modelling analysis and mixer performance simulation are presented in the following sections.

2. On-chip HTS mixer design

Figure 1 shows the schematic of the presented monolithic HTS THz mixer, where the THz CP antenna, diplexer, and bias-tee are integrated with the HTS Josephson junction on a single chip to form a full HTS receiver front-end. Under the harmonic mixing operation mode, the THz signal coupled into the junction via the CP antenna is down-converted into an intermediate frequency (IF) signal after mixing with a high-order harmonic of a local oscillator (LO) pumping signal at the Ka band (32–38 GHz). The on-chip diplexer and bias-tee networks are utilized to achieve good transmission and isolation of the LO, IF and DC biasing signals. Figure 2(a) shows the design layout of the monolithic mixer device integrated on a piece of $10 \times 10\,\mathrm{mm}^2$ MgO (dielectric constant ε_r: 9.63) substrate with a thickness of 0.5 mm. The yellow coloured layer is gold (electrical conductivity σ: $4.561 \times 10^7\,\mathrm{S\,m^{-1}}$) thin film, which is deposited on a HTS $YBa_2Cu_3O_7$ (YBCO) layer with the same pattern. The THz CP antenna lies in the upper right corner of the mixer chip (see the pink dashed box), and an anti-reflective (AR) Parylene ($\varepsilon_r = 2.62$) coated silicon (Si, $\varepsilon_r = 11.68$) lens is attached on the backside for achieving highly directional radiation. A coplanar waveguide (CPW) diplexer is designed to achieve effective transmission and isolation of the LO and IF signals, and it consists of a seventh-order stepped-impedance lowpass filter and a three-order capacitive-gap coupled resonator bandpass filter. A coplanar bias-tee based on a resistor–capacitor

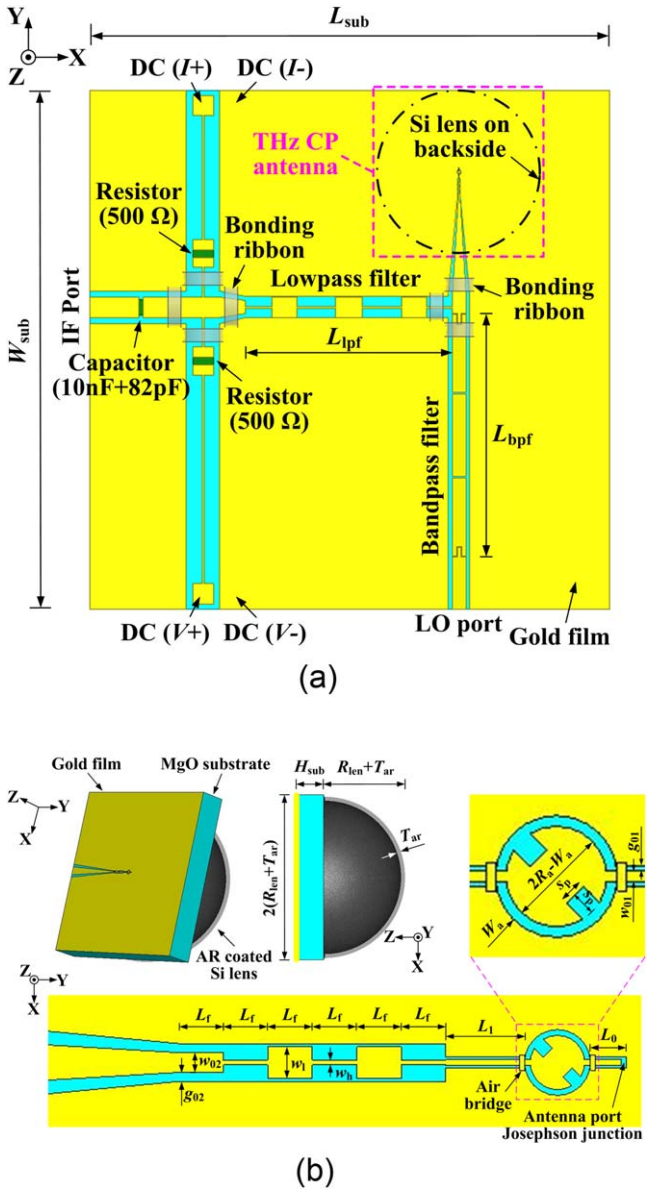

Figure 2. (a) Design layout of the presented monolithic HTS THz mixer; (b) geometry of the THz CP antenna with a Josephson junction integrated at its port. (Structural parameters: $L_{sub} = W_{sub} = 10$ mm, $H_{sub} = 0.5$ mm, $R_{len} = 1.5$ mm, $T_{ar} = 77\ \mu$m, $L_{lpf} = 3.98$ mm, $L_{bpf} = 4.69$ mm, $R_a = 40\ \mu$m, $W_a = 7\ \mu$m, $s_p = 16\ \mu$m, $w_{01} = 7\ \mu$m, $g_{01} = 3\ \mu$m, $w_{02} = 24\ \mu$m, $g_{02} = 11\ \mu$m, $w_h = 6\ \mu$m, $w_1 = 38\ \mu$m, $L_f = 54\ \mu$m, $L_1 = 96\ \mu$m, and $L_0 = 44\ \mu$m.)

network and high impedance CPW lines is designed to separate the DC bias and IF signals. Four DC pads are created for applying the four-point method (*I*+, *V*+, *I*-, *V*-) to measure the current–voltage characteristics (IVCs) of the HTS Josephson junction. Gold bonding ribbons are utilized for those CPW networks to suppress the unwanted coupled-slotline (CSL) mode [14]. Furthermore, considering the junction dynamic resistance value (usually of the order of a few tens of Ω), the diplexer and bias-tee are designed to be matched to 50 Ω.

The presented mixer integrates a novel CP antenna to couple the THz radiation into the HTS Josephson junction with enhanced signal coupling efficiency and polarization

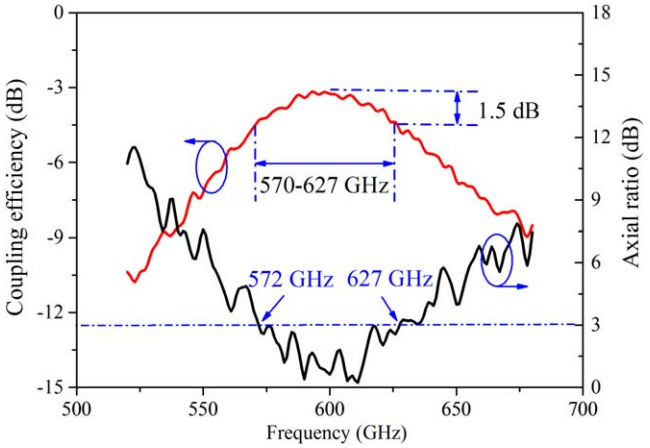

Figure 3. Simulated coupling efficiency and axial ratio of the THz CP antenna.

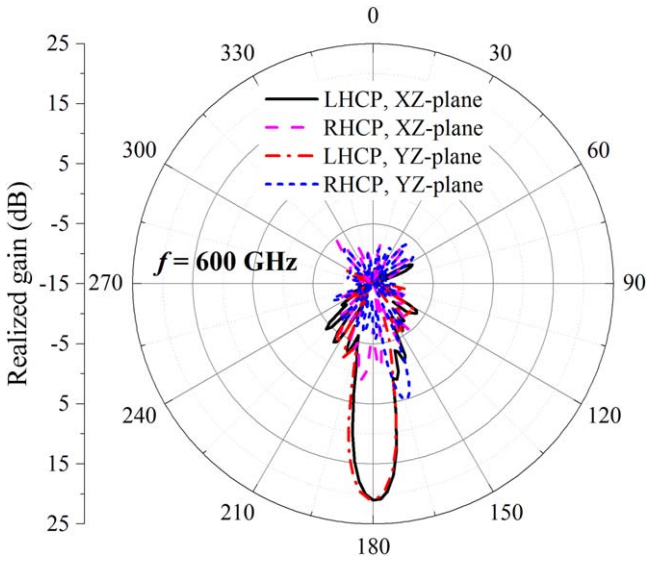

Figure 4. Simulated radiation pattern of the THz CP antenna at 600 GHz.

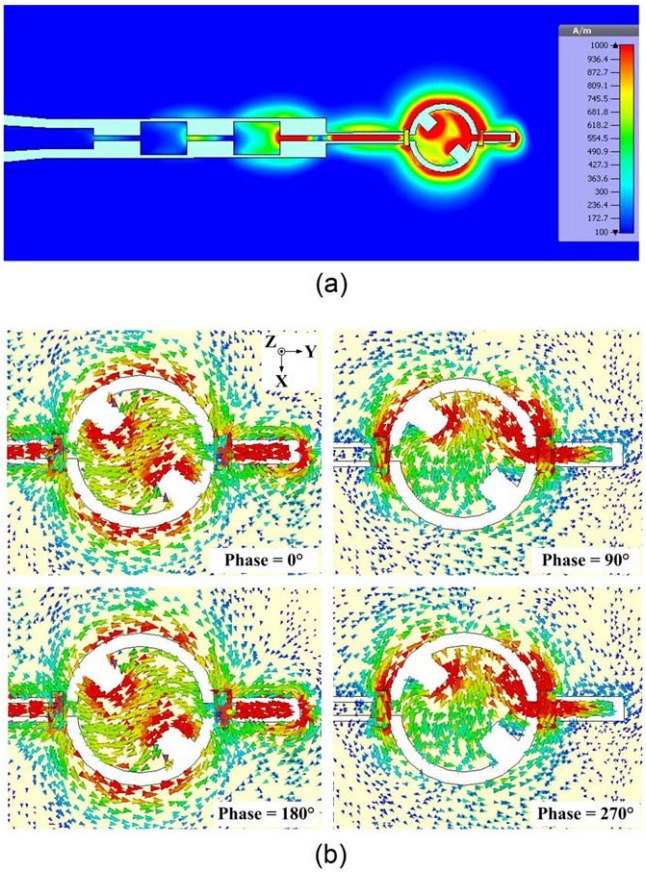

Figure 5. Simulated surface electric current distribution on the THz CP antenna at 600 GHz: (a) current amplitude; (b) current vector at different phases.

orientation flexibility. Figure 2(b) shows the geometry of the designed THz CP antenna including the impedance matching and isolation networks. The main radiator is a modified ring-slot thin film structure loaded with two perturbed square notches at its diagonal corners. Good CP radiation can be realized by adjusting the notch dimensions to handle the magnitude and phase relationships for two orthogonal linearly polarized (LP) field modes. Two gold air bridges are used to suppress the excitation of the undesired CSL mode resulting from the asymmetrical discontinuities introduced by notch loading. The HTS Josephson junction is located at the antenna port, and due to its low normal resistance R_n (typical value: 5 Ω), a 50 Ω CPW line transformer is utilized to minimize the impedance mismatch between the junction and the ring-slot antenna. On left side of the slot antenna is a CPW isolation network consisting of a fifth-order stepped-impedance choke filter to prevent the THz electric current from leaking onto the microwave ports.

3. Electromagnetic modelling analysis

After careful design and optimization through electromagnetic (EM) simulations, the final device structural parameters are obtained as shown in the caption of figure 2. Figures 3–7 show the EM analysis results of the monolithic integrated CP antenna-coupled HTS THz mixer. For CP antenna simulation, since YBCO film has a higher surface resistance than that of the gold film at the THz frequency band, the gold/YBCO layers are simplified as a gold film alone in the model. For monolithic circuit simulation, the gold/YBCO layers are assumed to be a perfect electrical conductor considering the superconductivity of YBCO at low microwave frequency range. A coupling efficiency η_c [9] is defined for the antenna to quantify its capability of coupling THz radiation into the HTS Josephson junction. Through simulation with Computer Simulation Technology (CST) software, it is found that, as shown in figure 3, the antenna has a high coupling efficiency achieving −3.1 dB at the resonant frequency of 600 GHz, and a 1.5 dB operating bandwidth of 570–627 GHz. The good results are attributed to an effective design for minimizing impedance mismatch loss, where the optimized antenna input resistance of 20 Ω at 600 GHz is relatively low, closer to the junction normal resistance (assumed as 5 Ω here), than the antennas in earlier works

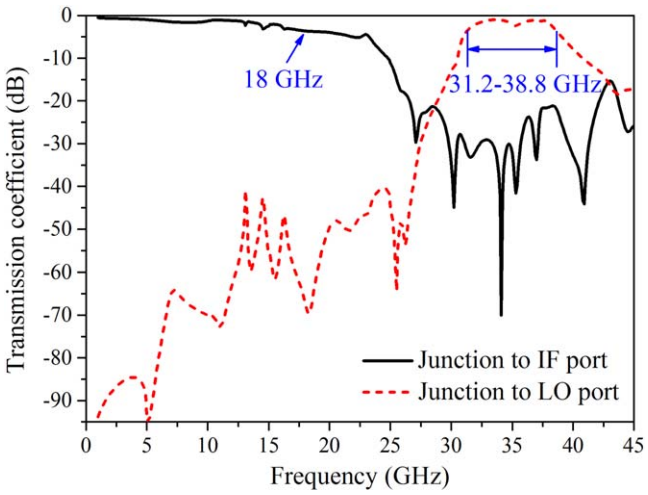

Figure 6. Simulated transmission coefficients from the Josephson junction to the LO and IF ports.

[8–11]. Figure 3 also shows the axial ratio characteristics in the negative Z direction. It is found that the THz antenna exhibits very good CP radiation with the axial ratio less than 3 dB over a frequency band from 572 to 627 GHz. Figure 4 is the simulated radiation pattern of the antenna at 600 GHz, and it shows a highly directional left-handed circularly polarized (LHCP) radiation. The radiation pattern exhibits very good symmetry in the XZ and YZ planes, and the side-lobe and cross-polarization (right-handed circular polarization) levels are all below −15 dB. The LHCP-realized gain of the THz antenna is around 20–21 dB over the whole operating frequency band.

Figure 5 shows the simulated surface electric current distribution on the THz CP antenna at 600 GHz. Seen from figure 5(a), the THz current has been effectively blocked by the isolation network from leaking to the leftmost end of the CPW line (for microwave signal transmission). Furthermore, a current valley is observed at the right end of the fifth-order stepped-impedance choke filter, which indicates that the left end of the ring-slot antenna can be regarded as virtually 'open' after an approximately half-wavelength CPW line (see 'L_1' in figure 2). Consequently, the field modes of the ring-slot antenna would not be influenced by the CPW isolation work. It should be emphasized that although there are some electric currents on the CPW lines, they do not contribute to THz radiation due to the mutual cancellation effect. Figure 5(b) shows the current–vector distribution at the phases of 0°, 90°, 180° and 270°, respectively. Obviously, the THz antenna radiates a LHCP wave towards the negative Z direction.

Figure 6 shows the simulated transmission coefficients from the Josephson junction to the LO and IF ports, respectively, which are obtained by using High Frequency Structural Simulator (HFSS) software. Clearly, a bandpass frequency response is observed for the LO signal transmissions, which have a 3 dB passband from 31.2 to 38.8 GHz, and a lowpass response with a 3 dB cutoff frequency up to 18 GHz for the IF transmission. Furthermore, the monolithic integrated circuit exhibits very good port isolation characteristics, achieving more than 20 dB for the LO and 40 dB for the IF signals, respectively. Figure 7 shows the simulated electric current distribution at the frequencies of 35 GHz and 6.5 GHz, which further clarifies the good signal transmission and isolation performance of the monolithic HTS THz mixer.

4. HTS Josephson junction mixer simulation and discussion

With the aim of validating the concept of design, active device modelling (after passive EM simulation) is carried out to evaluate the frequency conversion performance of the monolithic HTS THz mixer. The simulation method was recently developed by our group and has been described in detail in [15]. The method combines Keysight Advanced Design System (ADS) software with an imported Verilog-A model of the Josephson junction to model the full HTS monolithic microwave integrated circuit (MMIC) mixer, which has previously been successfully applied for modelling a Ka band HTS MMIC receiver [16]. Considering its powerful capability and high accuracy in analyzing the HTS Josephson devices that contain complicated peripheral networks (e.g. the matching and filter circuits), we have applied this approach to model the monolithic integrated CP antenna-coupled HTS THz harmonic mixer presented in this paper.

Based on the EM analysis results described above, an equivalent circuit model is established for the HTS THz mixer device as shown in figure 8. The current biasing, RF, LO and IF links are connected in parallel with the resistively-shunted HTS Josephson junction. A bandpass filter BPF_1 is used to describe the antenna performance in coupling THz radiation, which has an insertion loss of 3.1 dB at the central frequency of 600 GHz and a 1.5 dB passband bandwidth of 570–627 GHz. The left side of BPF_1 is matched to the junction normal resistance R_n and the right side matched to the RF source impedance Z_{RF} (i.e., the free-space wave impedance). Another bandpass filter BPF_2 (with a 3 dB passband from 31.2 to 38.8 GHz) is introduced between the LO source and the Josephson junction, which features insertion losses of 1.5 dB at 35 GHz and 40 dB at 26.8 GHz, respectively. In addition, a lowpass filter LPF (3 dB passband: 0–18 GHz) is utilized to describe the IF transmission characteristics, which has insertion losses of 0.5 dB at 1 GHz and 32 dB at 35 GHz, respectively. Both sides of the BPF_2 and LPF are matched to 50 Ω. A capacitor is included to prevent the bias current from leaking into the IF link. The DC, THz, LO and IF signals are well isolated from each other through these equivalent filters and capacitors.

Although the circuit design and modelling are applicable for different types of HTS Josephson junctions, the mixer device simulation here will be based on our step-edge junction characteristics. Figure 9 shows the simulated DC IVCs of the presented HTS THz mixer (assume $T = 40$ K, where the junction characteristics were extensively measured in previous work [9, 10]). Clearly, the unpumped HTS Josephson junction exhibits a typical resistively-shunted junction (RSJ) behaviour (see black curves). Under THz illumination or LO pumping, the junction critical current I_c is partly suppressed

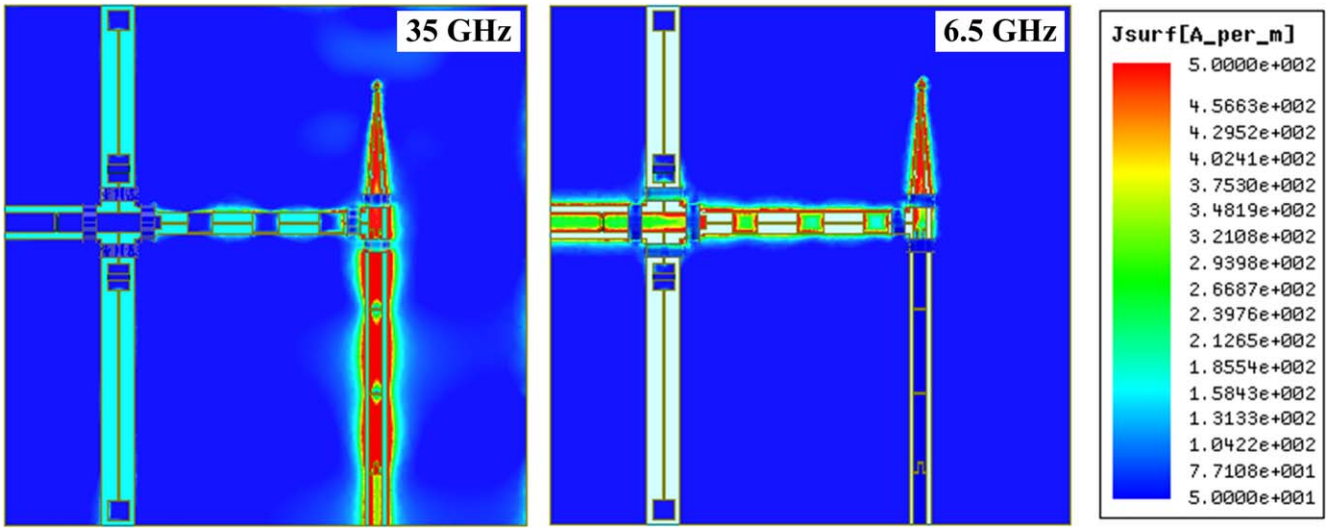

Figure 7. Simulated electric current distribution on the monolithic integrated circuit at the frequencies of 35 GHz (LO) and 6.5 GHz (IF).

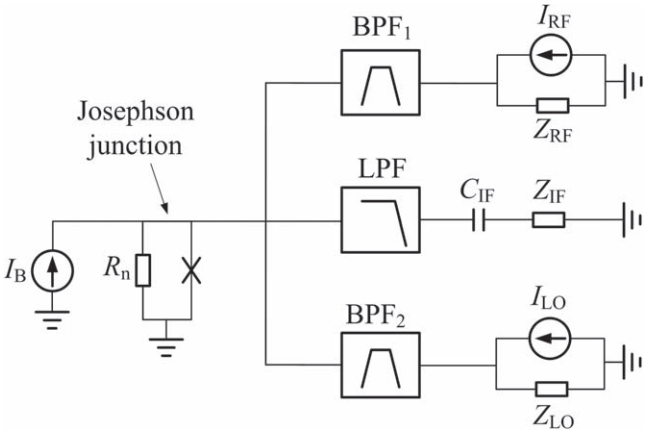

Figure 8. Equivalent circuit model of the presented monolithic HTS THz mixer device ($R_n = 5\,\Omega$, $Z_{RF} = 377\,\Omega$, $Z_{LO} = Z_{IF} = 50\,\Omega$, $C_{IF} = 10.082$ nF).

and the suppression increases with an increase in the source current I_{RF} or I_{LO}. Moreover, there are a series of Shapiro steps induced in the pumped IVCs shown in figure 9(a). As predicted by the Josephson voltage–frequency equation [17]: $V_n = n\Phi_0 f_{RF}$ (where n is an integer, Φ_0 is the magnetic flux quantum, and f_{RF} is the signal frequency), the voltage of the first induced Shapiro step is located at exactly 1.24 mV for the THz pumping at 600 GHz. The Shapiro steps induced by LO pumping are less visible in figure 9(b) due to a much lower frequency (36.9375 GHz) thus are small steps in a large voltage scale. In the simulation, the Josephson junction parameters ($R_n = 5\,\Omega$ and unpumped $I_c = 310\,\mu$A) are extracted from the measured results of the previous mixer described in [10]. Using the same junction characteristics can provide a fair comparison of mixing performance between this new design and previous devices. The I_c and R_n values are typical ones for our developed HTS step-edge junctions operating at 40 K.

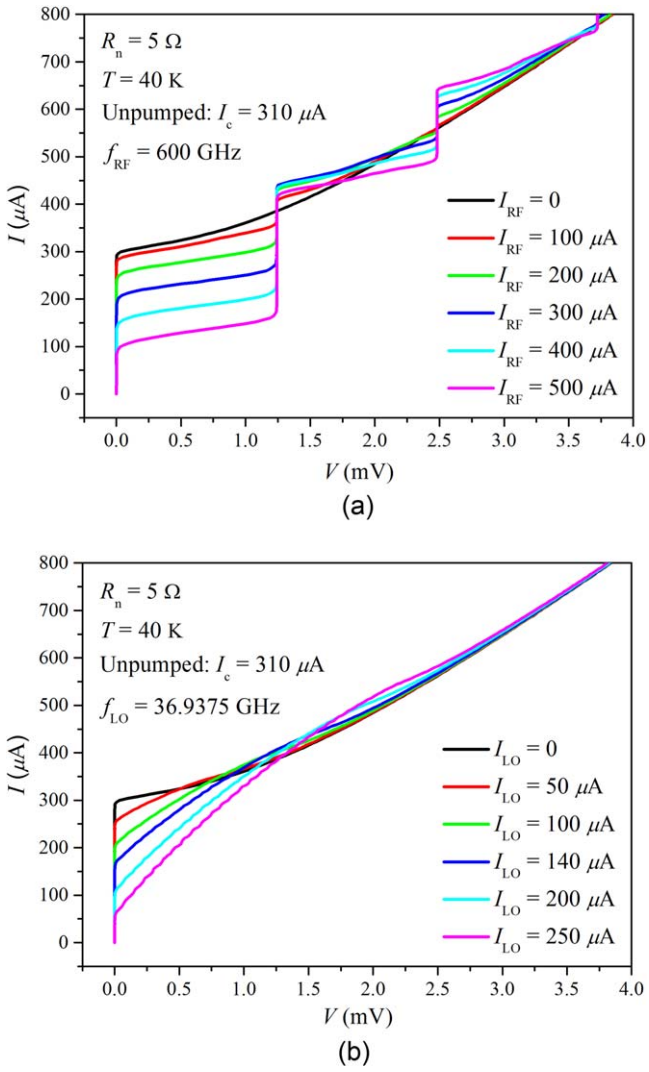

Figure 9. Simulated DC IVCs of the Josephson junction under (a) THz illumination and (b) LO pumping.

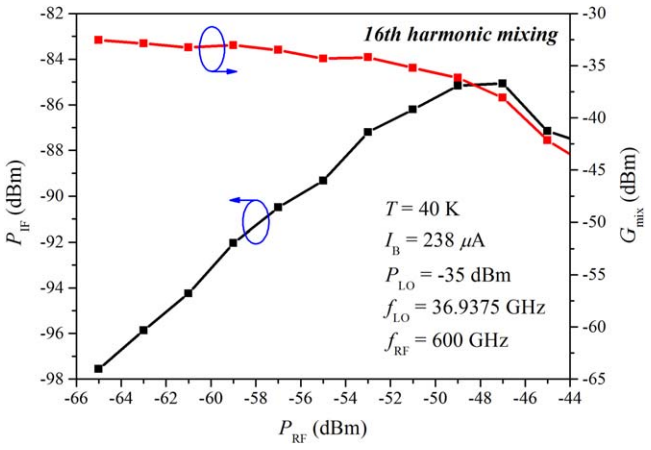

Figure 10. Simulated IF output power P_{IF} and mixer conversion gain G_{mix} versus the THz input power P_{RF}.

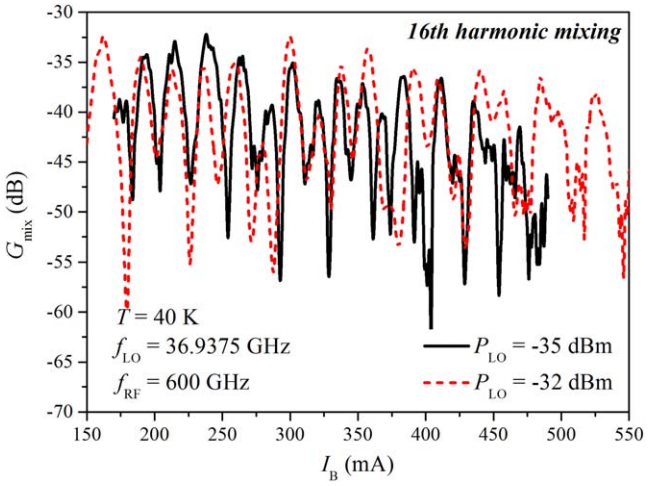

Figure 11. Simulated mixer conversion gain G_{mix} versus the bias current I_B for different LO pumping power P_{LO}.

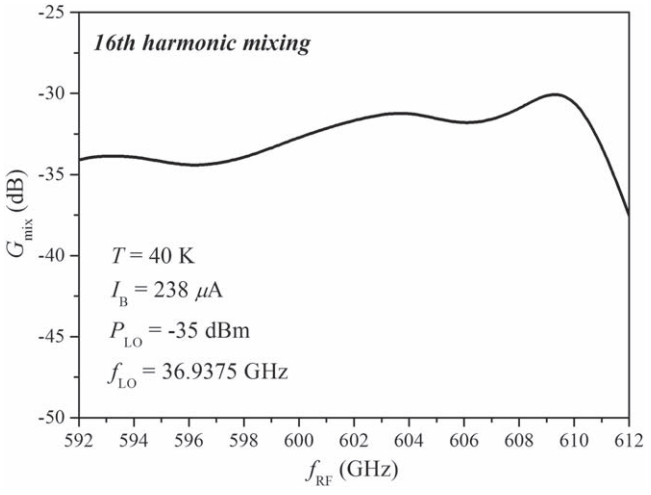

Figure 12. Simulated frequency response of the HTS THz mixer.

Figures 10–12 show the simulated frequency down-conversion performance of the monolithic HTS THz mixer at temperature of 40 K. A 600 GHz signal is down-converted to a 9 GHz IF signal when mixing with the 16th harmonic of an LO pumping signal at 36.9375 GHz. Figure 10 shows the simulated relationship of the IF output power P_{IF} versus THz input power P_{RF}, where the mixer exhibits good linearity at a lower P_{RF} range and then tends to saturate when P_{RF} is increased to near the LO power P_{LO}. The maximum mixer conversion gain G_{mix} (i.e. P_{IF}/P_{RF}) is about −33 dB and the 1 dB gain compression point is at $P_{RF} = -53$ dBm.

Figure 11 shows the bias current (I_B) dependence of the mixer conversion gain. The G_{mix} versus I_B relationship exhibits a strong modulation phenomenon with a number of resonant peaks appearing. This has been observed in a previous experiment [8] and is believed to result from the Shapiro steps induced by LO pumping; the P_{IF} minima occur at integer multiples or harmonics of the LO frequency f_{LO}, although might not at every value [11]. Furthermore, it is found from figure 11 that the mixer has a relatively wide bias current range (more than 200 μA at $P_{LO} = -35$ dBm) which further increases as the LO power rises.

Figure 12 shows the simulated frequency response of the mixer at the 600 GHz band. Under the 16th harmonic mixing at optimal I_B and P_{LO}, the mixer conversion gain is around −32.5 dB over a wide operating bandwidth of 592–611 GHz for RF and 1–20 GHz for IF, respectively. The minor fluctuation in the frequency response trace mainly results from a slight mismatch between the junction dynamic resistance and the input impedance of the IF lowpass filter (matched to 50 Ω).

The achieved mixer conversion gain is around 17 dB higher than that of our previous experimentally demonstrated HTS harmonic mixer [10]. However, it should be mentioned that this large improvement is a theoretical result. To validate the simulation method and more accurately estimate the performance improvement for the proposed new mixer, the same full circuit simulation method has been applied to analyze our previous broadband HTS THz mixer [10] with the same Josephson junction parameters (I_c, R_n) as that of the new monolithic mixer. Figure 13 shows the simulated and

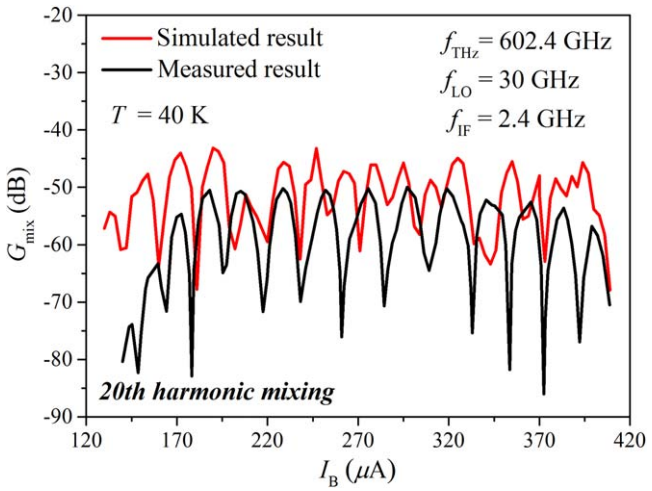

Figure 13. Measured and simulated results for a previous broadband HTS THz mixer reported in [10].

measured results of the conversion gain G_{mix} versus bias I_B for the demonstrated broadband HTS mixer in [10]. The theoretical and experimental results are in good agreement; both display a similar modulation behaviour with a similar current period. The result has validated the effectiveness of the presented simulation method for the HTS Josephson junction THz mixers. From figure 13, the simulated conversion gain is ∼−43 dB, about 6–7 dB higher than the measured one. The discrepancy is believed to mainly come from the extra transmission losses caused by resistive connections and discontinuities for non-monolithic integration of the broadband HTS harmonic mixer. These effects have not been included in the simulation. The new full monolithic integrated HTS mixer (including the bias-tee and diplexer) should reduce the losses associated with resistive connections and discontinuities, although a precise estimation of such an improvement is difficult without an experimental result. Nevertheless, ignoring the improvement by full on-chip circuit integration, there is still another ∼10 dB gain (deducting 6–7 dB from the 17 dB gain improvement) for the presented new mixer. The 10 dB gain comes from better signal coupling of the new THz CP antenna design (∼5 dB higher antenna coupling efficiency) and a lower harmonic order (∼5 dB, estimated from an earlier result in [11]). Conservatively speaking, a minimum of 10 dB gain improvement has been obtained from this new design of an all-inclusive monolithic CP antenna-coupled HTS THz harmonic mixer compared to the best reported results.

5. Conclusion

A novel monolithic integrated CP antenna-coupled HTS Josephson junction THz harmonic mixer is presented in this paper. The mixer has compact features, such that all its relevant components are integrated on a single $10 \times 10\,mm^2$ chip, which provides more efficient signal coupling, thus low loss, and it exhibits enhanced polarization orientation flexibility in coupling THz radiation. A full device design, modelling analysis and performance evaluation are provided in detail. Superior performance is demonstrated by simulation, an increase of at least 10 dB in conversion gain compared to the previously demonstrated HTS mixer with identical Josephson junction characteristics. The large improvement in performance is attributed to fact that the all-inclusive monolithic HTS circuit removes the resistive connection losses between components and has more efficient signal coupling and isolation for the RF, LO and IF ports. Such a new concept of a monolithic HTS THz mixer will have huge potential for ultra-sensitive and ultrahigh bitrate THz wireless applications.

ORCID iDs

Xiang Gao https://orcid.org/0000-0002-6108-2551

References

[1] Schneider T 2014 Ultrahigh-bitrate wireless data communications via THz-links; possibilities and challenges *J. Infrared Millimeter THz Waves* **36** 159–79
[2] Ducournau G, Szriftgister P, Pavanello F, Peytavit E, Zaknoune M, Bacquet D, Beck A, Akalin T, Lampin J-F and Lampin J-F 2015 THz communications using photonics and electronic devices: the race to data-rate *J. Infrared Millimeter THz Waves* **36** 198–220
[3] Chen J, Myoren H, Nakajima K, Yamashita T and Wu P H 1997 Mixing at terahertz frequency band using $YBa_2Cu_3O_{7-\delta}$ bicrystal Josephson junctions *Appl. Phys. Lett.* **71** 707–9
[4] Shimakage H, Uzawa Y, Tonouchi M and Wang Z 1997 Noise temperature measurement of YBCO Josephson mixers in millimeter and submillimeter waves *IEEE Trans. Appl. Supercond.* **7** 2595–8
[5] Harnack O, Darula M, Scherbel J, Heinsohn J-K, Siegel M, Diehl D and Zimmermann P 1999 Optimization of a 115 GHz waveguide mixer based on an HTS Josephson junction *Supercond. Sci. Technol.* **12** 847–9
[6] Scherbel J, Darula M, Harnack O and Siegel M 2002 Noise properties of HTS Josephson mixers at 345 GHz and operating temperatures at 20 K *IEEE Trans. Appl. Supercond.* **12** 1828–31
[7] Malnou M, Feuillet-Palma C, Ulysse C, Faini G, Febvre P, Sirena M, Olanier L, Lesueur J and Bergeal N 2014 High-T_c superconducting Josephson mixers for terahertz heterodyne detection *J. Appl. Phys.* **116** 074505
[8] Du J, Weily A R, Gao X, Zhang T, Foley C P and Guo Y J 2016 HTS step-edge Josephson junction terahertz harmonic mixer *Supercond. Sci. Technol.* **30** 024002
[9] Gao X, Zhang T, Du J, Weily A R, Guo Y J and Foley C P 2017 A wideband terahertz high-T_c superconducting Josephson-junction mixer: electromagnetic design, analysis and characterization *Supercond. Sci. Technol.* **30** 095011
[10] Gao X, Du J, Zhang T, Guo Y J and Foley C P 2017 Experimental investigation of a broadband high-temperature superconducting terahertz mixer operating at temperatures between 40 and 77 K *J. Infrared Millimeter THz Waves* **38** 1357–67
[11] Du J, Pegrum C, Gao X, Weily A R, Zhang T, Guo Y J and Foley C P 2017 Harmonic mixing using a HTS step-edge Josephson junction at 0.6 THz frequency *IEEE Trans. Appl. Supercond.* **27** 1500905
[12] Foley C P, Mitchell E E, Lam S K H, Sankrithyan B, Wilson Y M, Tilbrook D L and Morris S J 1999 Fabrication and characterisation of YBCO single grain boundary step edge junctions *IEEE Trans. Appl. Supercond.* **9** 4281–4
[13] Gao X, Du J, Zhang T and Guo Y J 2017 Noise and conversion performance of a high-T_c superconducting Josephson junction mixer at 0.6 THz *Appl. Phys. Lett.* **111** 192603
[14] Lee J, Lee H, Kim W, Lee J and Kim J 1999 Suppression of coupled-slotline mode on CPW using air-bridges measured by picosecond photoconductive sampling *IEEE Microw. Guided Wave Lett.* **9** 265–7
[15] Zhang T, Pegrum C, Du J and Guo Y J 2016 Simulation and measurement of a Ka-band HTS MMIC Josephson junction mixer *Supercond. Sci. Technol.* **30** 015008
[16] Zhang T, Gao X, Wang W, Du J, Pegrum C and Guo Y J 2017 A 36 GHz HTS MMIC Josephson mixer—simulation and measurement *IEEE Trans. Appl. Supercond.* **27** 1502405
[17] Duzer T V and Turner C W 1999 *Principles of Superconductive Devices and Circuits* (Upper Saddle River, NJ: Prentice Hall)